Applied Catalysis B: Environmental 97 (2010) 135–141

Contents lists available at ScienceDirect

Applied Catalysis B: Environmental

journal homepage: www.elsevier.com/locate/apcatb

# Effects of electrolyte on the electrocatalytic activities of $RuO_2$/Ti and Sb–$SnO_2$/Ti anodes for water treatment

Soonhyun Kim [a], Sung Kyu Choi [b], Bok Young Yoon [c], Sang Kyoo Lim [a,*], Hyunwoong Park [b,**]

[a] Division of Nano-Bio Technology, Daegu Gyeongbuk Institute of Science and Technology (DGIST), Daegu 704-230, Republic of Korea
[b] School of Physics and Energy Science, Kyungpook National University, Sankyuk 3, Bukgu, Daegu 702-701, Republic of Korea
[c] Plant Engineering Team, Sejong Plant, Daegu 702-260, Republic of Korea

ARTICLE INFO

*Article history:*
Received 29 December 2009
Received in revised form 5 March 2010
Accepted 24 March 2010
Available online 31 March 2010

*Keywords:*
$RuO_2$/Ti
Sb–$SnO_2$/Ti
NaCl
$Na_2SO_4$
Water treatment

ABSTRACT

The study of high efficiency electrochemical water treatment systems is of great importance in contributing to a sustainable water supply. In this study, we prepared $RuO_2$/Ti and Sb–$SnO_2$/Ti electrodes and investigated their electrocatalytic activities for the oxidation of water and three model substrates (methylene blue, acid orange 7, and 4-chlorophenol) in two supporting electrolytes: NaCl vs. $Na_2SO_4$. Irrespective of the electrolyte, the particulate $RuO_2$/Ti anode was found to oxidize water at ca. 0.8 V lower potential ranges with significantly higher currents than the cracked-mud type of Sb–$SnO_2$/Ti, indicating that the latter is more suitable for substrate oxidation. In the system of Sb–$SnO_2$/Ti anode–stainless steel cathode couple, the degradation rates of all the substrates were highly enhanced in NaCl, whereas their complete oxidation (i.e., $CO_2$ evolution) occurred more markedly in $Na_2SO_4$. Additional detailed experimental results indicated that the relative superiority of Sb–$SnO_2$/Ti over $RuO_2$/Ti for treating the model substrates depended greatly on the employed supporting electrolytes, and that the superiority particularly vanished when NaCl was used as the electrolyte. Using this electrolyte, active chlorine species-mediated indirect reactions seemed to occur at both anodes, while in the $Na_2SO_4$ electrolyte, the surface-specific reaction occurred. Finally, surface analysis and diverse electrochemical experiments were performed to compare both anodes in a more quantitative way and to investigate the effect of the electrolytes on the electrocatalytic activities of the anodes.



## 1. Introduction

Electrochemical advanced oxidation processes (EAOPs) have received great attention as one of the most promising technologies for the treatment of water containing recalcitrant organic pollutants [1–4]. The electrochemical oxidation of substrates begins with the generation of radical species (e.g., $HO^{\bullet}$) that are sorbed chemically and/or physically at the anode (Eq. (1)) [2]. The formation of the radicals and their subsequent interactions with the anode surface and the substrates, therefore, are significantly affected both by the anode catalyst materials [5–12] and supporting electrolytes [13–18].

Great efforts have been made to develop highly efficient and robust anodes for water treatment [1–12]. In general, anodes are classified into two types according to their electrochemical behaviors [2,3,19]. The first is a so-called active anode. This type of anode undergoes changes in the oxidation state of its catalytic components during electrochemical processes, such as oxidation ($M^{x+}$ to $M^{(x+2)+}O$) by the chemi-sorbed hydroxyl radical (Eq. (2)), reduction ($M^{(x+2)+}O$ to $M^{x+}$) during the substrate (R) oxidation (Eq. (3)), and disproportionation of MO (Eq. (4)). The latter competes with substrate oxidation (Eq. (3) vs. Eq. (4)), inevitably lowering the treatment efficiency of the substrate and producing oxygen at low potentials (low oxygen evolution potential anode). The active anodes include Pt [7,10,14,20,24], $IrO_2$ [8,12,21], $RuO_2$ [6,9,10,12,22], stainless steel [19], etc.

$$M + H_2O \rightarrow M + HO^{\bullet} + H^+ + e^- \quad (1)$$

$$M + HO^{\bullet} \rightarrow (M\text{–}HO^{\bullet}_{chem}) \rightarrow MO + H^+ + e^- \quad (2)$$

$$MO + R \rightarrow M + RO \quad (3)$$

$$2MO \rightarrow 2M + O_2 \quad (4)$$

$$M + HO^{\bullet} \rightarrow (M\text{–}HO^{\bullet}_{phys}) \quad (5)$$

$$(M\text{–}HO^{\bullet}_{phys}) + R \rightarrow M + H_2O + CO_2 \quad (6)$$

$$2(M\text{–}HO^{\bullet}_{phys}) \rightarrow 2M + H_2O_2 \quad (7a)$$

$$2(M\text{–}HO^{\bullet}_{phys}) \rightarrow 2M + O_2 + 2H^+ + e^- \quad (7b)$$

* Corresponding author. Tel.: +82 53 430 8432; fax: +82 53 430 8443.
** Corresponding author. Tel.: +82 53 950 7371; fax: +82 53 952 1739.
*E-mail addresses:* limsk@dgist.ac.kr (S.K. Lim), hwp@knu.ac.kr (H. Park).

0926-3373/$ – see front matter © 2010 Elsevier B.V. All rights reserved.
doi:10.1016/j.apcatb.2010.03.033

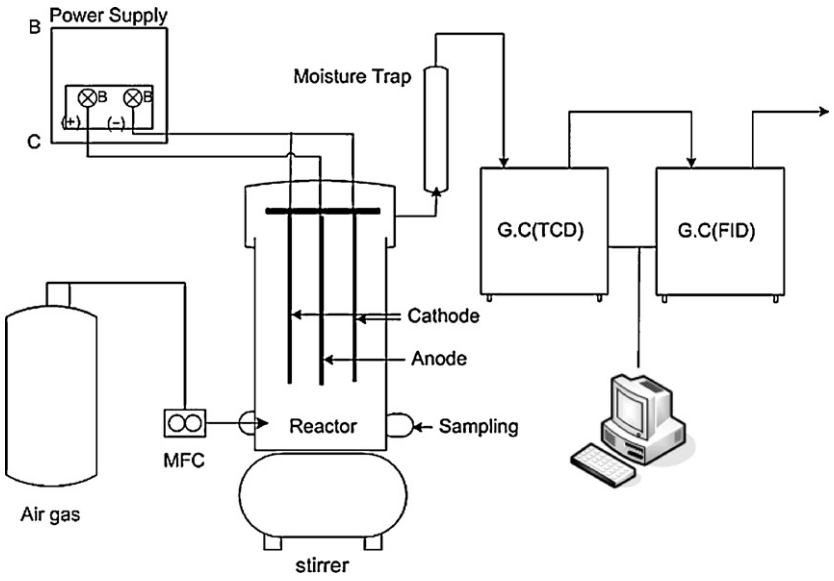


**Scheme 1.** Schematic illustration of the experimental set-up.

On the other hand, the non-active anode type binds the hydroxyl radical physically and rather loosely on its surface catalytic sites during the initial electrolysis stage (Eq. (5)). Hence, the hydroxyl radical can be readily transferred to interfacial substrates, leading to their complete oxidation (Eq. (6)). In addition, the production of hydrogen peroxide (Eq. (7a)) competes kinetically with the oxygen evolution (Eq. (7b)), lowering the oxygen evolution rate and thus requiring a higher potential to achieve measurable oxygen evolution (high oxygen evolution potential anode). The non-active anodes are $PbO_2$ [7,11,14,23], $SnO_2$ [14,24], boron-doped diamond [4,11,15,19], etc.

The selection of electrolyte is also very important in determining overall treatment efficiency. Although organic substrates are primarily degraded by the adsorbed hydroxyl radical, the in situ generated chemical oxidants from the supporting electrolytes can contribute to substrate degradation, irrespective of the anode type. For example, in the presence of NaCl electrolyte, active chlorine species such as $Cl^{\bullet}$, $Cl_2^{\bullet-}$, $HOCl/ClO^-$ are formed from the oxidation of chloride ions at the anode surface [13–15,18,25]. In the $Na_2SO_4$ electrolyte, $SO_4^{\bullet-}$ can be produced, but in a very limited case (i.e., at BDD) [13,15,25].

Several studies have been carried out regarding the comparison of electrochemical treatment performances between active and non-active anodes or between NaCl and $Na_2SO_4$ [13,15,18]. Yet detailed and systematic studies on the effects of the electrolyte on the performance of active and non-active anodes have not been investigated thoroughly. With this in mind, we prepared two kinds of anode ($RuO_2$/Ti as active anode [6,9,10,12] and Sb–$SnO_2$/Ti as non-active anode [5,10,26–29]), and compared their electrochemical behaviors and performances in the oxidation of three model substrates: methylene blue, acid orange 7, 4-chlorophenol in two supporting electrolytes: NaCl vs. $Na_2SO_4$.

## 2. Experimental

### 2.1. Preparation of anodes

A Ti metal sheet was cut to a rectangle with a dimension of 2 cm × 7 cm and thickness of 1.5 mm. This Ti plate was polished with SiC paper (400–2000 grit) and etched in a concentrated HCl solution followed by sequentially washing with acetone and deionized water. The pretreated Ti plates were dipped into coating solutions that consisted of 0.16 M $SnCl_2{\cdot}2H_2O$ and 0.04 M $SbCl_3$ in ethanol for Sb–$SnO_2$/Ti and 0.2 M $RuCl_3$ in ethanol for Ti/$RuO_2$; they were then slowly withdrawn from the solutions. To obtain a thicker and more robust catalytic film, the above procedure was repeated 15 cycles, and the Ti plates were heated at 450 °C for 5 min during each cycle and for 1 h during the final cycle (Fig. S1 in Supplementary Material). The mass of coated materials was estimated to be about 1.5–2.2 mg/cm$^2$. In the case of Sb–$SnO_2$/Ti, the absence of Sb (i.e., $SnO_2$/Ti) caused high anode resistance, significantly lowering the electrocatalytic activities (Fig. S2 in Supporting Material).

### 2.2. Electrochemical reactions

The experimental set-up for the electrochemical reactions is illustrated in Scheme 1. The electrode couple is composed of a single anode (Sb–$SnO_2$/Ti or $RuO_2$/Ti) with an active area of 20 cm$^2$ (2 cm × 5 cm, both sides) in contact with an electrolyte and two plates of the same-size stainless steel (SS) cathode that faced both sides of the anode with a separation distance of 3 mm. The couple was immersed in NaCl or $Na_2SO_4$ electrolyte (100 ml) with one of the model pollutants (methylene blue (MB), acid orange 7 (AO-7), and 4-chlorophenol (4-CP)) at a given concentration. Air was continuously purged through the electrolyte as a background carrier gas during the electrochemical reaction. A constant cell voltage ($E_{cell}$) or current ($I_{cell}$) was applied to the electrodes with a DC power supply (E3633A, Agilent). The reactor was sealed from the atmosphere and the headspace gas was forced to flow at a given rate (100 ml/min) by regulating the background carrier gas through a mass flow controller (5850E, Brooks).

### 2.3. Analytical methods

A given volume of the headspace gas was intermittently carried into a gas chromatograph (GC, HP6890N) equipped with a thermal conductivity detector (TCD) for hydrogen and a flame ionization detector (FID) for carbon dioxide. The aqueous phase products and intermediates were identified and quantified using a UV–vis spectrophotometer (Varian) and using a high performance liquid chromatography (HPLC, Agilent) equipped with a C18 column. The HPLC eluent was composed of 60 vol.% water (0.1 vol.% phosphoric acid) and 40 vol.% acetonitrile at a flow rate of 1 ml/min.

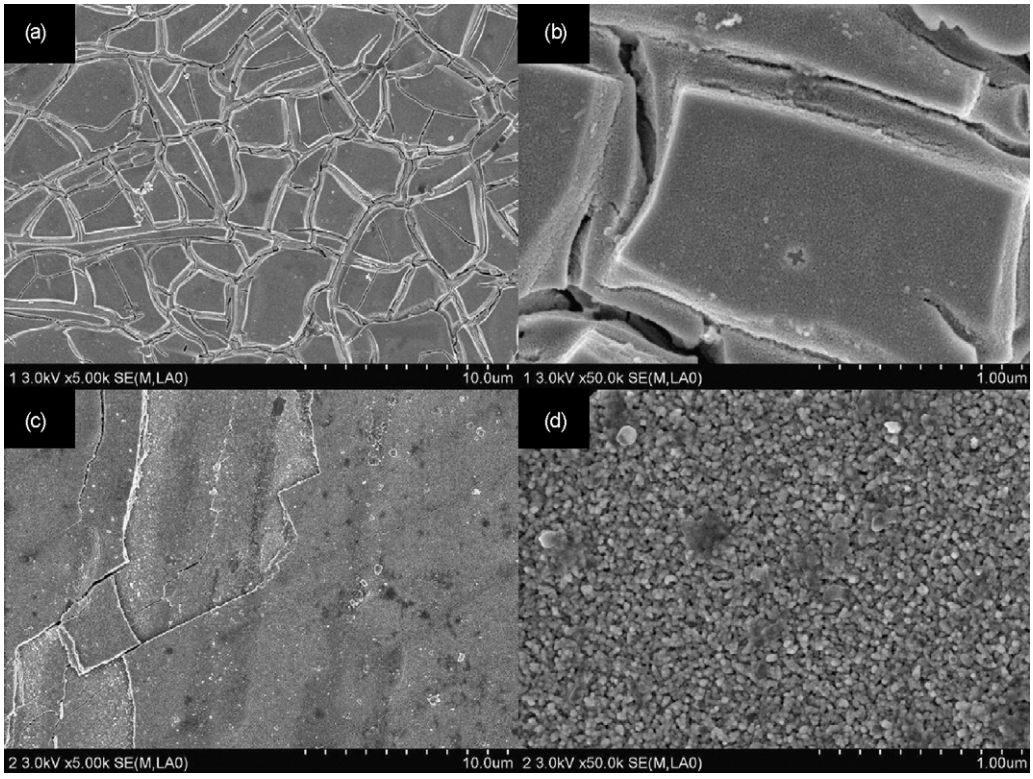


**Fig. 1.** SEM images of Sb–$SnO_2$/Ti (a and b) and $RuO_2$/Ti (c and d) electrodes.

The cyclic voltammetry (CV) was conducted to investigate the electrochemical behavior of as-prepared anodes using a potentiostat (VSP, Princeton Applied Research). A Pt mesh and a standard Ag/AgCl were used as the counter electrode and the reference electrode, respectively. Electrolyte was composed of 1 M $H_2SO_4$ with either 60 mM NaCl or 30 mM $Na_2SO_4$.

The surface morphological images of as-prepared anodes were obtained using a field emission scanning electron microscope (FE-SEM, Hitachi S-4200). XRD patterns were obtained with an X-ray diffractometer (Rigaku D/MAX-2500, 18 kV) using Cu-$K_{a1}$ radiation.

## 3. Results and discussion

### 3.1. Comparison of $RuO_2$/Ti and Sb–$SnO_2$/Ti electrodes in water electrolysis

Fig. 1 shows the SEM images of $RuO_2$/Ti and Sb–$SnO_2$/Ti electrode surfaces. Both electrodes have cracked, fractured surfaces exposing larger electrocatalytic micro-surfaces to electrolytes. The marked difference between the two is that $RuO_2$/Ti is composed of very fine particles, whereas Sb–$SnO_2$/Ti does not show any grain boundaries and appears as if the grains are dissolved to mud. This cracked-mud structure is typically observed when Sb–$SnO_2$/Ti is prepared by thermal decomposition [29]. The X-ray diffraction measurement was conducted for $RuO_2$/Ti and Sb–$SnO_2$/Ti electrodes as well (Fig. 2). It was determined that both metal oxides were rutile-structured. In the case of Sb–$SnO_2$/Ti, no peaks for antimony (or its oxide) were detected, probably due to its mixing with the $SnO_2$ structure, as reported elsewhere [27,29]. The sharp peaks originated from Ti base metal.

To investigate the electrochemical behaviors as a function of electrolyte, the cyclic voltammograms of both electrodes were studied in a NaCl and a $Na_2SO_4$ solution (Fig. 3). The $RuO_2$/Ti electrode has a large amount of Faradaic anodic currents (forward scan) at >∼1.2 V vs. Ag/AgCl (∼1.4 V vs. NHE at pH 0) [6,10], which are ascribed to the water oxidation reaction (Eq. (8a)).

$$2H_2O \rightarrow O_2 + 4H^+ + 4e^-; \quad E^\circ = 1.23\,\text{V vs. NHE} \tag{8a}$$

$$O_2 + 4H^+ + 4e^- \rightarrow 2H_2O \tag{8b}$$

Although the forward scans generate similar water oxidation current values, the reverse scans have different behaviors particularly at 0.9 and 1.2 V vs. Ag/AgCl. At these potentials, $RuO_2$/Ti in NaCl has apparent cathodic peaks while that in $Na_2SO_4$ does not. Hence, the cathodic peaks should be associated with the reduction of active chlorine species generated and adsorbed in the forward scan, which are likely to be hypochlorous acid/hyperchlorite ($HClO/OCl^-$) (Eq. (9)), chlorine radical ($Cl^\bullet$) (Eq. (10)), and/or dichloride radical anion ($Cl_2^{\bullet -}$) (Eq. (11)) [13,18].

$$HClO + H^+ + e^- \rightarrow 0.5Cl_2 + H_2O; \quad E^\circ = 1.63\,\text{V vs. NHE} \tag{9a}$$

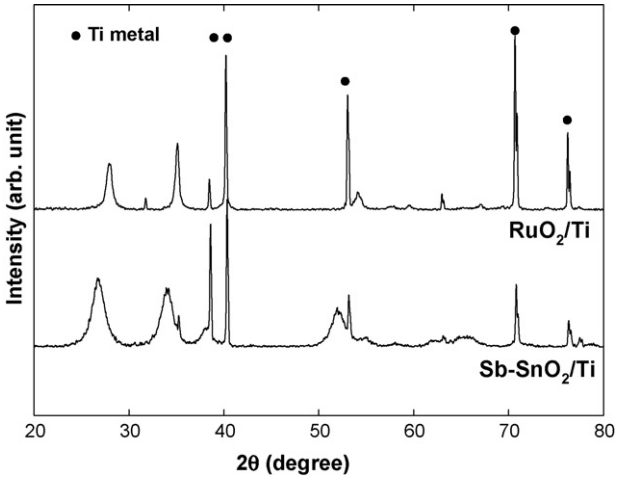


**Fig. 2.** XRD patterns of Sb–$SnO_2$/Ti and Ti/$RuO_2$/Ti electrodes.

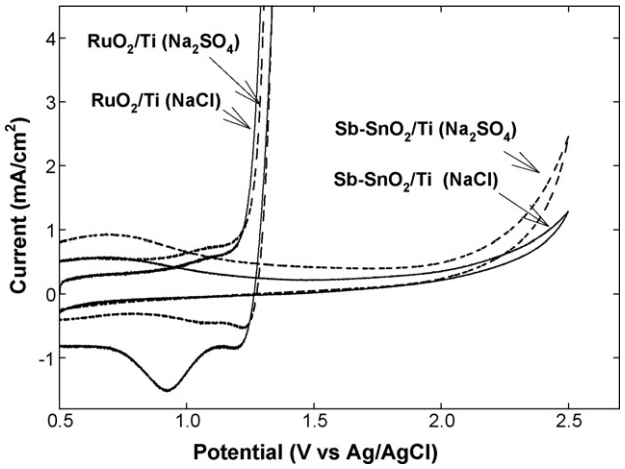


**Fig. 3.** Cyclic voltammograms of Sb–$SnO_2$/Ti and Ti/$RuO_2$/Ti electrodes (1 $cm^2$) in 1 M $H_2SO_4$/60 mM NaCl or 1 M $H_2SO_4$/30 mM $Na_2SO_4$ electrolytes at scan rates of 20 mV/s.

$$HClO + H^+ + 2e^- \rightarrow Cl^- + H_2O; \quad E^\circ = 1.49\,V \text{ vs. NHE} \tag{9b}$$

$$ClO^- + H_2O + 2e^- \rightarrow Cl^- + 2OH^-; \quad E^\circ = 0.90\,V \text{ vs. NHE} \tag{9c}$$

$$Cl^\bullet + e^- \rightarrow Cl^-; \quad E^\circ = 2.4\,V \text{ vs. NHE} \tag{10}$$

$$Cl_2^{\bullet -} + e^- \rightarrow 2Cl^-; \quad E^\circ = 2.0\,V \text{ vs. NHE} \tag{11}$$

Careful comparison of the reduction potentials of the chlorine species indicates that the peak at 1.2 V vs. Ag/AgCl (1.4 V vs. NHE) is likely to correspond to the reduction of dichloride radical anion (Eq. (11)) or adsorbed oxygen (Eq. (8b)), while the other peak at 0.9 V vs. Ag/AgCl (1.1 V vs. NHE) to the reduction of hypochlorous acid (Eq. (9a) and (9b)). We exclude the possibilities of the chlorine radical reduction (Eq. (10)) due to its very short life time and of the hypochlorite reduction (Eq. (9c)) due to thermodynamic limit and circum-neutral acid dissociation constant of HClO ($pK_a$ = 7.36) in strongly acidic electrolyte (pH ~ 1). In the case of $Na_2SO_4$, a minor reduction peak at 1.22 V vs. Ag/AgCl is observed, which seems to be the reduction of adsorbed oxygen that is produced during the water oxidation (Eq. (8b)).

Conversely, irrespective of the supporting electrolyte employed, Sb–$SnO_2$/Ti has a very wide non-Faradaic current region up to ca. 2.0 V and less steep cathodic current generation curves thereafter [10,29]. This indicates that water oxidation at Sb–$SnO_2$/Ti is significantly inhibited and occurs at a much elevated potential, around 0.8 V higher than that at $RuO_2$/Ti. It is of note that the reverse scans in NaCl and $Na_2SO_4$ exhibit no specific cathodic current peak, likely because only the tiny amount of oxygen at the surface is reduced and the surface interaction of the supporting electrolyte ions is highly inhibited. The similarity between both electrolytes further indicates the electrochemical reaction at Sb–$SnO_2$/Ti is non-specific and indirect (i.e., generation of radical species from the surface and their diffusion toward bulk electrolyte; homogeneous-like reaction).

Fig. 4 shows the dc-powered electrochemical behaviors of $RuO_2$/Ti and Sb–$SnO_2$/Ti anodes coupled with stainless steel cathodes in NaCl and $Na_2SO_4$ electrolytes. This kind of anode–cathode coupled two-electrode system is very practical, applicable, and even scientifically interesting since the effects of anodic reaction on cathodic reaction (or vice versa) can be studied in a single cell [16–18]. As shown in Fig. 4a, the $RuO_2$/Ti–SS couple begins to generate cell current ($I_{cell}$) at >2.0 V along with higher $I_{cell}$ values with increasing cell potential ($E_{cell}$), whereas Sb–$SnO_2$/Ti–SS has lower $I_{cell}$ values despite the similar current-onset potential. When comparing the supporting electrolytes, one

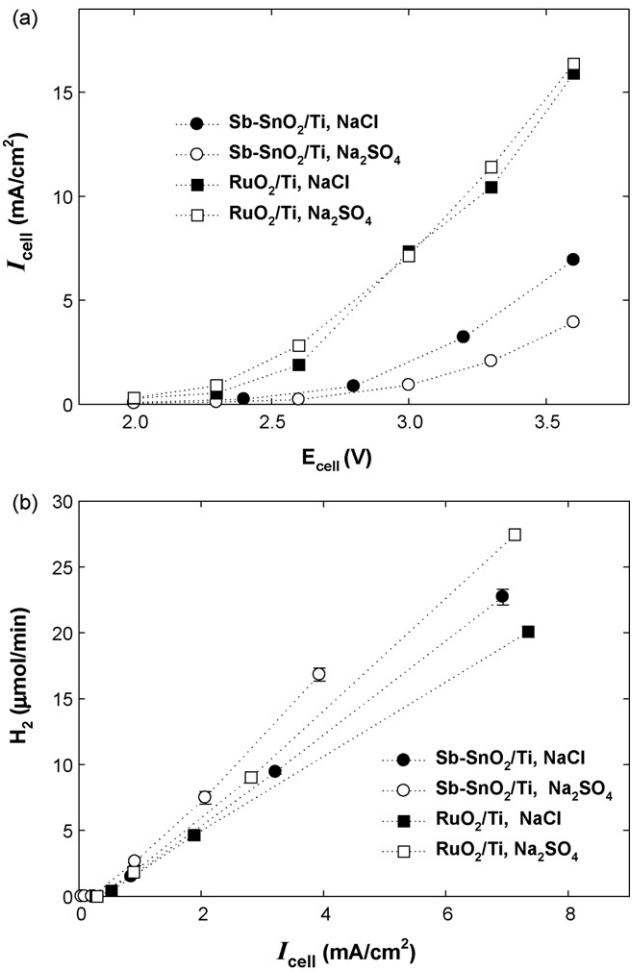


**Fig. 4.** (a) Effects of applied cell voltages ($E_{cell}$) on cell currents ($I_{cell}$) and (b) hydrogen production rates as a function of $I_{cell}$s at Sb–$SnO_2$/Ti anode–stainless steel (SS) cathode and $RuO_2$/Ti anode–SS cathode couples in NaCl (60 mM) and $Na_2SO_4$ (30 mM) electrolyte.

finds that NaCl is more effective in generating $I_{cell}$ than $Na_2SO_4$ at Sb–$SnO_2$/Ti ($I_{cell,chloride} > I_{cell,sulfate}$) whereas $I_{cell}$ values are quite similar between both in the case of $RuO_2$/Ti ($I_{cell,chloride} \sim I_{cell,sulfate}$) (Table 1).

We have also monitored the simultaneous hydrogen production from water (Fig. 4b) occurring at the SS cathode with the following equation.

$$2H_2O + 2e^- \rightarrow H_2 + 2OH^-; \quad E^\circ = 0\,V \text{ vs. NHE} \tag{12}$$

Since $I_{cell}$ is equal to the anodic current ($I_a$) as well as the cathodic current ($I_c$) (i.e., $I_{cell} = I_a = I_c$), and a greater $I_c$ implies a higher hydrogen production rate ($r_H$) at the cathode, $I_{cell}$ should show a positive correlation with $r_H$ [17]. This further suggests that the hydrogen production rate in NaCl ($r_{H,chloride}$) must be greater than that in $Na_2SO_4$ ($r_{H,sulfate}$) for the case of using the Sb–$SnO_2$/Ti anode (i.e., $r_{H,chloride} > r_{H,sulfate}$) and similar when $RuO_2$/Ti anode is used (i.e., $r_{H,chloride} \sim r_{H,sulfate}$). Comparison of the cell currents (Fig. 4a) and the hydrogen production rate (Fig. 4b), however, shows that irrespective of the anodes, $r_H$ is always lower in NaCl. Therefore, the cathodic current efficiency for the hydrogen production (CCE, defined as $r_H/I_{cell} \times 100\%$) also becomes to be reduced in NaCl (Table 1). This reduction might be ascribed to an electron-shuttling effect of active chlorine species between the anode and the cathode in NaCl electrolyte (e.g., $Cl^-/Cl_2^-$; see Eqs. (13)–(15)) [17,18].

$$Cl^- \rightarrow Cl^\bullet + e^- \quad \text{(anode)} \tag{13}$$

**Table 1**
Electrocataltyic activities of $RuO_2$/Ti and Sb–$SnO_2$/Ti anodes in NaCl (C) and $Na_2SO_4$ (S) electrolytes.

| Anode | $I$[a] (mA/cm$^2$) | $I_{cell}$[b] (mA) | $r_H$[b] (μmol/min) | CCE (%)[c] | $k_{obs}$ (min$^{-1}$) (S) | | | $k_{obs}$ (min$^{-1}$) (C) | | |
|---|---|---|---|---|---|---|---|---|---|---|
| | | | | | MB | AO7 | 4CP | MB | AO7 | 4CP |
| $RuO_2$ | C > S at 1.3 V | C ~ S | 2.07(C) 3.73(S) | 31.4(C) 56.5(S) | 0.01 | – | – | 0.25 | – | – |
| Sb–$SnO_2$ | S > C at 2.5 V | C > S | 3.19(C) 4.07(S) | 48.4(C) 61.7(S) | 0.04 | 0.02 | 0.02 | 0.14 | 1.59 | 0.61 |

[a] Current densities in a three-electrode system. Voltages were given with respect to Ag/AgCl.
[b] Currents and hydrogen production rates in a two-electrode system. Stainless steel was used as the cathode.
[c] Cathodic current efficiency for hydrogen production (%) = {$H_2$ production rate (μmol/min) × 2}/{$I_{cell}$ (C/s) × 60} × 100%. Estimated from data in Fig. 4b.

$$Cl^{\bullet} + Cl^- \rightarrow Cl_2^{-} \quad \text{(bulk)} \tag{14}$$

$$Cl_2^{-} + e^- \rightarrow 2Cl^- \quad \text{(cathode)} \tag{15}$$

In other words, a certain fraction of electrons that flowed from the anode to the stainless steel cathode is consumed by oxidized chlorine species (e.g., $Cl_2^-$) dragged to the cathode, which results in a competitive reaction with water molecules for electrons (Eq. (12)) and consequently lowers the rate of hydrogen production. When the electron-shuttling effect is inhibited or minimized, however, the NaCl electrolyte should have the similar to or higher hydrogen production rates than the $Na_2SO_4$ (see below).

### 3.2. Electrocatalytic degradation of organic pollutants at Sb–$SnO_2$/Ti anode

In order to investigate the electrocatalytic activities of as-prepared anodes for organic pollutants, three model substrates were selected: methylene blue (MB, cation), acid orange 7 (AO7, anion), and 4-chlorophenol (4-CP, neutral). In addition, for a more complete understanding of the electrochemical process, the production of both hydrogen (from water) and carbon dioxide (from the substrates) were measured in situ while recording time-profiled substrate concentrations (Fig. 5). Immediately after applying a constant cell current of 5 mA/cm$^2$, MB of 20 μM was rapidly degraded by following apparent pseudo-first order kinetics ($-d[MB]/dt = k_{obs}[MB]$; $[MB]_t = [MB]_0 \exp(-k_{obs}t)$); at the same time hydrogen was produced and its concentration reached a plateau in a few minutes (Fig. 5a). The MB degradation accompanied evolution of carbon dioxide after around 10 min-electrolysis, which reached a peak in ca. 20 min and then declined. All these reactions were affected little by the solution pH (Fig. S3 in Supporting Material). It is obvious that the supporting electrolyte NaCl is far more effective in degrading MB than $Na_2SO_4$ by a factor of 3.5 despite the similar $CO_2$ evolution rates (Table 1).

The Sb–$SnO_2$/Ti anode was also tested for the electrocatalytic degradation of AO7 (100 μM) in NaCl and $Na_2SO_4$ electrolytes (Fig. 5b). Similarly to the MB electrolysis, AO7 underwent much faster degradation in NaCl by a factor of around 80 (Table 1) and its degradation was completed within 2 min despite 5-fold higher initial concentration as compared to MB (20 μM). It is of note, however, that a substantial amount of $CO_2$ was evolved in $Na_2SO_4$ whereas only the tiny amount was evolved in NaCl over the whole period of electrolysis. Finally, the electrocatalytic activity of Sb–$SnO_2$/Ti for 4-CP was evaluated as well (Fig. 5c). As in the cases of MB and AO7, the degradation of 4-CP was accelerated in the presence of NaCl by ca. 30 times in comparison with $Na_2SO_4$; yet the $CO_2$ evolution was significantly enhanced in $Na_2SO_4$. As for the hydrogen production in NaCl, it was higher in the initial phase and then declined to the same level of that in $Na_2SO_4$.

### 3.3. Comparison of NaCl vs. $Na_2SO_4$

The above three hybrid reactions have varying degrees of efficiency for the treatment of substrates and production of hydrogen (see Table 1). Nevertheless, it is obvious that all the degradation reactions of MB, AO7, and 4-CP were significantly enhanced in NaCl. In this electrolyte system, the water oxidation reaction (Eq. (8a)) was greatly inhibited such that the overall water splitting ratio ($H_2/O_2$) was around 40 (Fig S4 in Supplementary Material); instead, chloride was oxidized to active chlorine species such as $Cl^{\bullet}$, $Cl_2^{\bullet -}$, HOCl, and $ClO^-$. The substrates, therefore, can be degraded via hydrogen abstraction, electrophilic addition, or direct electron transfer reactions by the chlorine species. Among those reaction mechanisms, the electrophilic addition most likely occurs [17,18].

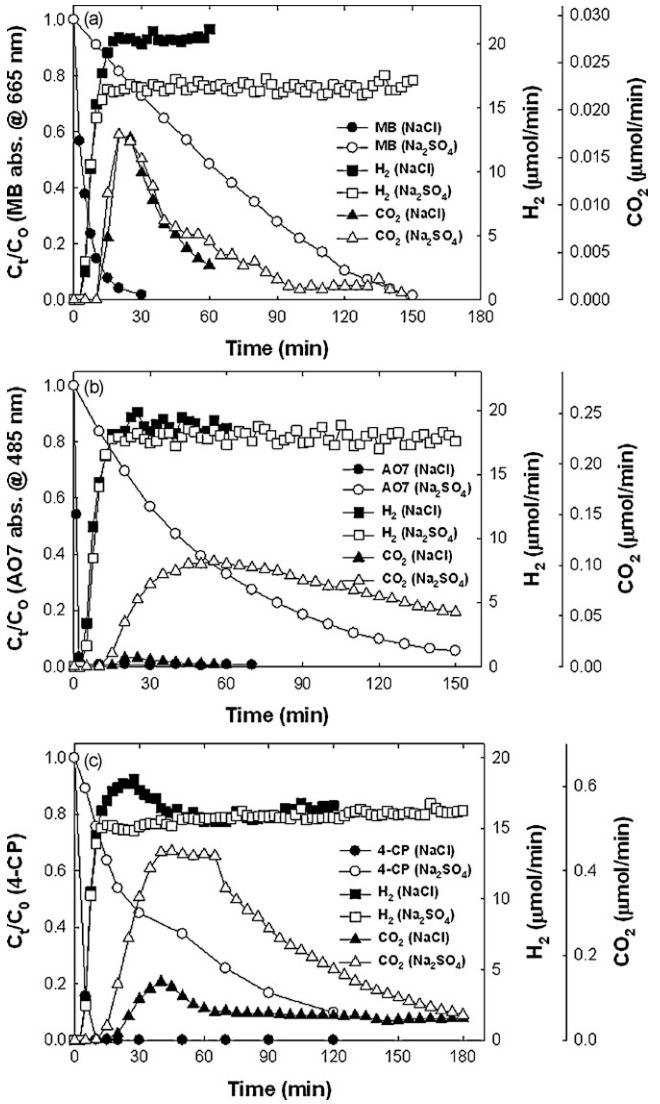


**Fig. 5.** Time-profiled decays of model substrates (a: methylene blue of 20 μM, b: acid orange 7 of 100 μM, c: 4-chlorophenol of 500 μM), evolutions of carbon dioxide, and simultaneous cathodic hydrogen productions at Sb–$SnO_2$/Ti anode–SS cathode couple in different electrolytes (NaCl vs. $Na_2SO_4$). $I_{cell}$ = 5 mA/cm$^2$; [NaCl] = 60 mM; [$Na_2SO_4$] = 30 mM.

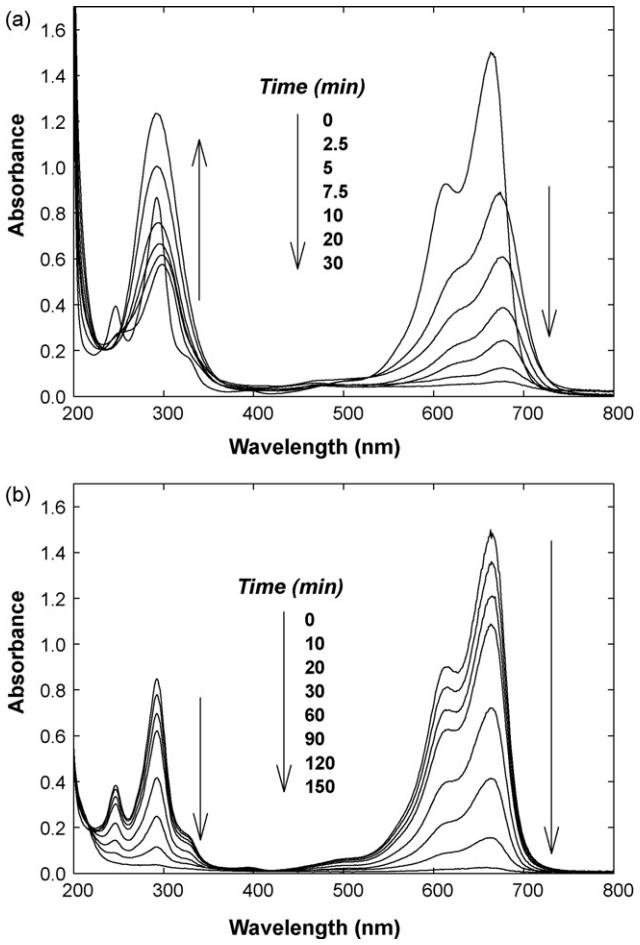


**Fig. 6.** Changes of UV–vis absorption spectra of methylene blue during its electrochemical oxidation in (a) NaCl and (b) $Na_2SO_4$ electrolytes. Experimental conditions identical to those of Fig. 5a.

This speculation is supported by the time-profiled UV–vis absorption spectra of MB during the course of its electrolysis in NaCl. As shown in Fig. 6a, as the absorbance at $\lambda \sim 290$ nm which is attributed to hypochlorite (or hypochlorous acid) increased, the MB absorption band ($\lambda = 665$ nm) was gradually red-shifted along with decreases in the absorbance. This red-shift should be caused by the formation of a complex between MB and the active chlorine species.

In the case of 4-CP, highly chlorinated phenols were observed (Fig. S5 in Supplementary Material), suggesting the presence of similar reaction pathway [16,18]. Accordingly, the degradation of substrates by the active chlorine species might be initiated via an addition of chlorine to substrates. Note that $k_{obs}$ is highly dependent on the chemical structure. For example, the degradation rates of hydroquinone and 2,4,6-trichlorophenol are ca. 5 and 4 times faster than phenol, respectively, whereas those of salicylic acid and benzoic acid are 2 and 250 times slower than phenol, respectively [18]. This indicated that chlorine and hydroxyl substituents enhance $k_{obs}$, while carboxyl substituent decreases it in comparison to phenol. In this study, the highly chlorinated phenol intermediates (2,4-dichlorophenol, 2,6-dichlorophenol, and 2,4,6-trichlorophenol) that are produced via the reaction of 4-CP and active chlorine species are degraded at higher rates than 4-CP by a factor of 2.4∼6.61, insignificantly affecting the degradation kinetics of 4-CP.

In the $Na_2SO_4$ system, no red-shifts of absorption bands for MB and AO7 were found, indicating the complex formation between the sulfate radical and the substrates did not happen (Fig. 6b). The degradation of 4-CP also showed no sulfate adducts as intermediates; instead, more hydroxylated intermediates (e.g., 4-chloro catechol) were transiently formed during the electrolysis (Fig. S6 in Supplementary Material). These suggest that substrates are likely to be directly oxidized either at the anode surface (Eq. (16)) or via reactions with the adsorbed sulfate radicals (Eqs. (17)) and/or hydroxyl radicals (Eqs. (18)) at the anode surface [13,18].

$$>Sb\text{–}SnO_2\text{–}R_{ads} \rightarrow >Sb\text{–}SnO_2(e^-)\text{–}R^+{}_{ads} \quad (16)$$

$$>Sb\text{–}SnO_2\text{–}SO_4{}^{2-}{}_{ads} \rightarrow >Sb\text{–}SnO_2(e^-)\text{–}SO_4{}^{\bullet -}{}_{ads} \quad (17a)$$

$$>Sb\text{–}SnO_2\text{–}SO_4{}^{\bullet -}{}_{ads} + R \rightarrow >Sb\text{–}SnO_2\text{–}SO_4{}^{2-}{}_{ads} + R^+ \quad (17b)$$

$$>Sb\text{–}SnO_2\text{–}H_2O_{ads} \rightarrow >Sb\text{–}SnO_2(e^-)\text{–}OH^{\bullet}{}_{ads} + H^+ \quad (18a)$$

$$>Sb\text{–}SnO_2\text{–}OH^{\bullet}{}_{ads} + RH \rightarrow >Sb\text{–}SnO_2(e^-) + ROH + H^+ \quad (18b)$$

Since the surface reactions (i.e., direct reactions) are largely influenced by substrate diffusion or migration from bulk solution toward the anode surface (i.e., heterogeneous-like reactions), the overall degradation rates of substrate in $Na_2SO_4$ should be limited. In NaCl, on the contrary, the active chlorine species are generated toward bulk solution and thus an indirect and homogeneous-like solution reaction of substrates would take place at higher rates than the surface reaction. However, since the solution reaction proceeds for all the bulk substrate and intermediate molecules at the same time, while the surface reaction occurs only for the adsorbed substrate and intermediate molecules, the more rapid and complete oxidation of the adsorbed molecules (i.e., $CO_2$ evolution) might occur despite the reduced overall degradation rate.

This conjecture was supported by the time-profiled $CO_2$ evolution graphs (Fig. 5). Although a minimal difference in $CO_2$ evolution was observed in MB electrolysis, the other two substrates (AO7, 4-CP) showed obviously much greater $CO_2$ evolution in $Na_2SO_4$. Furthermore, the $CO_2$ gas in the NaCl electrolyte began to evolve around the time that the parent substrates had almost completely degraded, whereas it was concurrently produced during the course of degradation of the parent substrates in $Na_2SO_4$. The delayed production of $CO_2$ in the NaCl electrolyte suggests that the production of chlorinated intermediates and their complete mineralization slowly occurred. We do not ignore the possible effect of pH on $CO_2$ evolution from electrolytes. In fact, the solution pH was raised from 6 to around 9 in NaCl electrolysis whereas it decreased down to 3∼4 in $Na_2SO_4$ electrolysis. These pH changes were similar to those in pure electrolysis (i.e., in the absence of substrates). Therefore a certain fraction of substrate carbon might remain as $HCO_3{}^-$ or $CO_3{}^{2-}$ in NaCl electrolyte, not leaving as gaseous $CO_2$. Yet their amounts should be minimal (Fig. S3 in Supplementary Material).

### 3.4. Comparison of $RuO_2$/Ti vs. Sb–$SnO_2$/Ti in MB electrolysis

The electrochemical degradation of organic substrates was significantly affected by the kind of electrocatalytic materials, and it has been reported that Sb–$SnO_2$/Ti is superior to $RuO_2$/Ti for degradation of organic compounds in water due to its high oxygen evolution potential [10]. However, the effects of electrocatalytic materials are different depending on the electrolytes employed. As compared in Fig. 7a, the MB degradation rates are very similar between $RuO_2$/Ti (active anode) and Sb–$SnO_2$/Ti (non-active anode) in NaCl electrolyte, whereas they are significantly different in $Na_2SO_4$. Furthermore, the dependence of the anode performance on the electrolyte persists for a wide range of operation cell currents from 5 to 25 mA/cm$^2$ (Sb–$SnO_2$/Ti (NaCl)∼$RuO_2$/Ti (NaCl); Sb–$SnO_2$/Ti ($Na_2SO_4$) ≫ $RuO_2$/Ti ($Na_2SO_4$)) (Fig. 7b). The reason seems to be related to the direct (heterogeneous) vs. indirect (homogeneous) reactions. As discussed in previous section, active chlorine species produced either from $RuO_2$/Ti or Sb–$SnO_2$/Ti

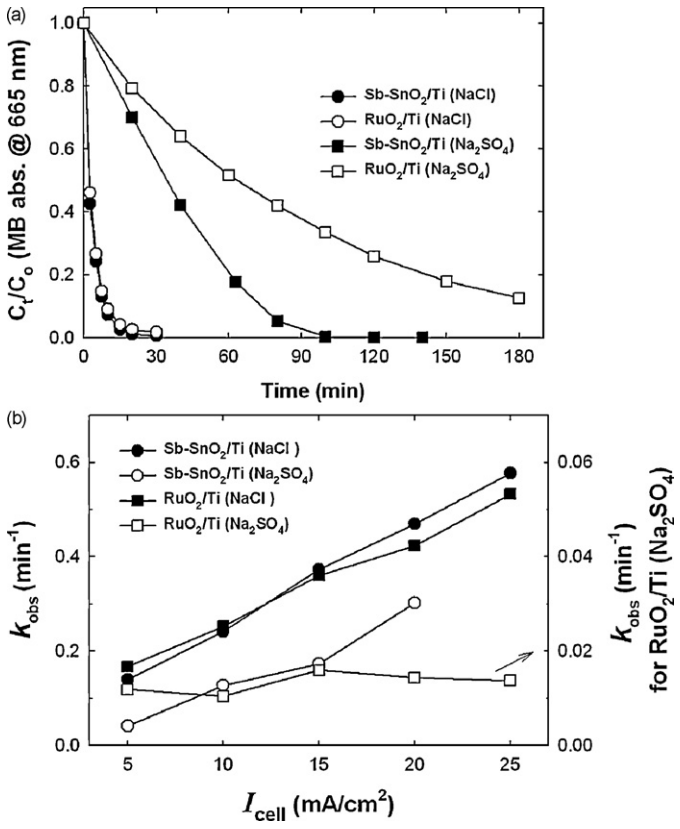


**Fig. 7.** (a) Comparison of Sb–$SnO_2$/Ti and $RuO_2$/Ti anodes for electrochemical degradation of methylene blue in NaCl and $Na_2SO_4$ electrolytes ($I_{cell}$ = 10 mA/cm$^2$). (b) Effects of $I_{cell}$ on the degradation kinetics ($k_{obs}$) of methylene blue at Sb–$SnO_2$/Ti anode–SS cathode couple and $RuO_2$/Ti–SS cathode couples in different electrolytes (NaCl vs. $Na_2SO_4$) [methylene blue]$_0$ = 50 μM; [NaCl] = 60 mM; [$Na_2SO_4$] = 30 mM.

are transported to bulk electrolyte away from the anode surface. Thus the surface and type of anode influences the degradation of substrate insignificantly. Conversely, the degradation reaction of substrates occurs primarily at the anode surface in $Na_2SO_4$; accordingly the degradation reaction should be greatly affected by the nature of electrocatalytic materials. The comparison of MB degradation rates ($k_{obs}$) in $RuO_2$/Ti–SS and Sb–$SnO_2$/Ti–SS systems makes the effect of electrocatalytic materials more obvious. As shown in Fig. 7b, $k_{obs}$ increased linearly with increasing the cell current density ($I_{cell}$) in both systems with NaCl electrolyte. In $Na_2SO_4$ electrolyte, however, Sb–$SnO_2$/Ti–SS still has the linear correlation between $k_{obs}$ and $I_{cell}$ whereas $RuO_2$/Ti–SS has no dependence on $I_{cell}$. Since Sb–$SnO_2$/Ti suppresses effectively the oxygen evolution rate, most of current applied to this anode is used for the MB oxidation, resulting in the linear correlation between $k_{obs}$ and $I_{cell}$. On the other hand, $RuO_2$/Ti as a good oxygen evolution electrocatalyst consumes most current for water oxidation, leading to no enhancement of $k_{obs}$ with increasing $I_{cell}$.

## 4. Conclusions

We have investigated the effects of supporting electrolytes on the electrocatalytic degradation of some selected organic substrates at active $RuO_2$/Ti and non-active Sb–$SnO_2$/Ti anodes. It has been found that despite equal importance, electrolytes are likely to more greatly influence the degradation kinetics of parent substrates and their mineralization to carbon dioxide than anodes in a wide range of operating cell currents. In this regard, application of electrochemical water treatment in the field should consider the selection of electrolytes as seriously as the preparation of anodes. Both anodes have different electrocatalytic activities and service lives in treating water pollutants; yet changing the electrolyte can minimize the difference.

## Acknowledgments

This research was supported by the DGIST basic program of the Ministry of Education, Science and Technology and by the Basic Science Research Program through the National Research Foundation of Korea (NRF) funded by the Ministry of Education, Science and Technology, Korea (No. 2009-0071350).

## Appendix A. Supplementary data

Supplementary data associated with this article can be found, in the online version, at doi:10.1016/j.apcatb.2010.03.033.

## References

[1] S. Trasatti, Electrochim. Acta 45 (2000) 2377–2385.
[2] C. Comninellis, Electrochim. Acta 39 (1994) 1857–1862.
[3] O. Simond, V. Schaller, C. Comninellis, Electrochim. Acta 42 (1997) 2009–2012.
[4] M. Panizza, G. Cerisola, Electrochim. Acta 51 (2005) 191–199.
[5] B. Correa-Lozano, C. Comninellis, A. De Battisti, J. Appl. Electrochem. 27 (1997) 970–974.
[6] T. Arikawa, Y. Murakami, Y. Takasu, J. Appl. Electrochem. 28 (1998) 511–516.
[7] J. Iniesta, E. Exposito, J. Gonzalez-Garcia, V. Montiel, A. Aldaz, J. Electrochem. Soc. 149 (2002) D57–D62.
[8] C.P. De Pauli, S. Trasatti, J. Electroanal. Chem. 538 (2002) 145–151.
[9] Y.J. Feng, X.Y. Li, Water Res. 37 (2003) 2399–2407.
[10] X.Y. Li, Y.H. Cui, Y.J. Feng, Z.M. Xie, J.D. Gu, Water Res. 39 (2005) 1972–1981.
[11] M. Panizza, G. Cerisola, Appl. Catal.B: Environ. 75 (2007) 95–101.
[12] M. Li, C.P. Feng, W.W. Hu, Z.Y. Zhang, N. Sugiura, J. Hazard. Mater. 162 (2009) 455–462.
[13] C. Comninellis, A. Nerini, J. Appl. Electrochem. 25 (1995) 23–28.
[14] F. Bonfatti, S. Ferro, F. Lavezzo, M. Malacarne, G. Lodi, A.D. Battisti, J. Electrochem. Soc. 147 (2000) 592–596.
[15] M. Murugananthan, S. Yoshihara, T. Rakuma, N. Uehara, T. Shirakashi, Electrochim. Acta 52 (2007) 3242–3249.
[16] H. Park, C.D. Vecitis, W. Choi, O. Weres, M.R. Hoffmann, J. Phys. Chem. C 112 (2008) 885–889.
[17] H. Park, C.D. Vecitis, M.R. Hoffmann, J. Phys. Chem. A 112 (2008) 7616–7626.
[18] H. Park, C.D. Vecitis, M.R. Hoffmann, J. Phys. Chem. C 113 (2009) 7935–7945.
[19] P. Canizares, F. Martinez, M. Diaz, J. Garcia-Gomex, M.A. Rodrigo, J. Electrochem. Soc. 148 (2002) D118–D124.
[20] B. Boye, M. Dieng, E. Brillas, Environ. Sci. Technol. 36 (2002) 3030–3035.
[21] X. Chen, G. Chen, P.L. Yue, J. Phys. Chem. B 105 (2001) 4623–4628.
[22] S. Ardizzone, G. Fregonara, S. Trasatti, Electrochim. Acta 35 (1990) 263–267.
[23] N.B. Tahar, A. Savall, J. Electrochem. Soc. 145 (1998) 3427–3434.
[24] S. Tanaka, Y. Nakata, T. Kimura, Yustiawati, M. Kawasaki, H. Kuramitz, J. Appl. Electrochem. 32 (2002) 197–201.
[25] S. Ferro, A. De Battisti, I. Duo, C. Comninellis, W. Haenni, A. Perret, J. Electrochem. Soc. 147 (2000) 2614–2619.
[26] F. Montilla, E. Morallon, J.L. Vazquez, J. Electrochem. Soc. 152 (2005) B421–B427.
[27] M. Seo, Y. Akutsu, H. Kagemoto, Ceram. Int. 33 (2007) 625–629.
[28] C. Borras, C. Berzoy, J. Mostany, J.C. Herrera, B.R. Scharifker, Appl. Catal. B: Environ. 72 (2007) 98–104.
[29] F. Montilla, E. Morallon, A. De Battisti, J.L. Vazquez, J. Phys. Chem. B 108 (2004) 5036–5043.